

Andrzej RYNIOWICZ¹, Konrad RYSZ², Łukasz BOJKO³

¹ State University of Applied Sciences in Nowy Sącz, Institute of Technology, 33-300 Nowy Sącz, Zamenhoffa 1A street, e-mail: andrzej@ryniewicz.pl

² Comarch Kraków, 31-864 Kraków, Jana Pawła II 39 street, e-mail: konrad.michal.rysz@gmail.com

³ AGH University of Science and Technology, Faculty of Mechanical Engineering and Robotics, Department of Machine Design and Maintenance, 30-059 Kraków, Mickiewicza 30 street, e-mail: lbojko@agh.edu.pl

Analysis of the accuracy of mapping in computed tomography**Abstract**

The aim of the study is to assess the accuracy of mapping the internal structure and shape of phantoms in computed tomography (CT) imaging, using reconstructive metrology and virtual measurements. The tests material is tomographic imaging of diagnostic phantoms: the head phantom used for monthly calibrations of computer tomographs and the specialized phantom for tests performed once a year. The Materialize Mimics computer program was used to measure the geometry of objects inside the phantoms and to measure the radiological density in the cross-sections of the tested patterns. It is a universal tool for assessing the accuracy of mapping in CT imaging. The results of the measurements were used to perform a complete statistical analysis. The values of standard deviations for the performed measurements did not exceed the limit value, which means that the tested tomograph meets the requirements for homogeneity of imaging and noise level specified in the Regulation of the Minister of Health. The proposed procedure is important for the target device, but can also be a tool for comparing the quality of different tomographs.

Key words: tomographic imaging, phantoms, measurements, radiological density, shape.

Analiza dokładności odwzorowania w tomografii komputerowej**Streszczenie**

Celem pracy jest ocena dokładności odwzorowania struktury wewnętrznej i kształtu fantomów w obrazowaniu tomografią komputerową (CT), z zastosowaniem metrologii rekonstrukcyjnej i pomiarów wirtualnych. Materiałem badań jest obrazowanie tomograficzne fantomów diagnostycznych: fantomu głowy używanego do comiesięcznych kalibracji tomografów komputerowych i fantomu specjalistycznego do testów wykonywanych raz w roku. Do pomiarów geometrii obiektów znajdujących się wewnątrz fantomów oraz pomiarów gęstości radiologicznej w przekrojach badanych wzorców wykorzystano program komputerowy Materialise Mimics. Stanowi on uniwersalne narzędzie do oceny dokładności odwzorowania w obrazowaniu CT. Wyniki pomiarów wykorzystano do przeprowadzenia pełnej analizy statystycznej. Wartości odchyłeń standardowych dla wykonanych pomiarów nie przekroczyły wartości granicznej, co oznacza, że badany tomograf spełnia wymogi odnośnie do jednorodności obrazowania i poziomu szumów, ujęte w Rozporządzeniu Ministra Zdrowia. Zaproponowana procedura jest istotna dla docelowego urządzenia, ale może również stanowić narzędzie do porównania jakości różnych tomografów.

Słowa kluczowe: obrazowanie tomograficzne, fantomy, pomiary, gęstość radiologiczna, kształt.

1. Introduction

High accuracy of mapping is a crucial issue of Computer Tomography (CT) because it is decisive in regards to diagnosis, determining treatment plan and, frequently, planning and progress of a surgery (Filippou, Tsoumpas, 2018; Higaki et al., 2020; Jahnke et al., 2019; Shim et al., 2020; Tino, Yeo, Leary, Brandt, Kron, 2019; Villarraga-Gomez, Herazo, Smith, 2019). The control test procedure for Computer Tomography x-ray scanners is based on the standards and regulations issued by the Minister of Health (PN-EN ISO 2919:2014-12; standard; PN-ISO 14146:2006 standard; PN-ISO 9978:1999 standard; Health Minister Regulation of 18th of February 2011 regarding safe application of ionizing radiation for all types of medical exposure, 2011). The most crucial parameters influencing quality of tomography mapping are: accuracy of mapping, spatial resolution capability, contrast, uniformity,

image distortions, thickness of a cross-section and efficiency of dose (Akpochafor et al., 2019; De Oliveira, Wenzel, Campos, Spin-Neto, 2017; Filippou, Tsoumpas, 2018; Ryniewicz, 2013; Sahbaee, Segars, Marin, Nelson, Samei, 2017; Si-Mohamed et al., 2018; Yasaka, 2017; Turek, Budzik, Przeszłowski, 2020). According to recommendations control tests for CAT scanner are performed cyclically and consist of analysis of imaging/mapping of master template models – phantoms (Bolstad, Flatabø, Aadnevik, Dalehaug, Vetti, 2018; Hermanek, Carmignato, 2017; Higaki et al., 2020; Jahnke et al., 2018; Si-Mohamed et al., 2018; Subhas et al., 2018; Wu et al., 2019; Yasaka et al., 2017). The phantoms are constructed from components varying in terms of geometry and construction materials the radiation absorption properties of which, expressed on Haunsfield scale (HU), corresponds with properties of human tissues (Ryniewicz et al., 2015; Ryniewicz, Ryniewicz, Bojko, 2019, Holmes, 2020; Haleem, Javaid, 2020).

The goal of this paper is to assess accuracy of mapping of an internal structure and shape of phantoms during computer tomography (CT) imaging through use of reconstructive metrology and virtual measurements.

2. The material and method

The object of the analysis consisted of the results of study of tomographic imaging performed for two phantoms: a head phantom and a specialized phantom, by using BrightSpeed 16 Power-Elite CAT scanner manufactured by General Electric Company in 2012 (Figure 1). This model is a 16-row, spiral CAT scanner in which circular motion of deflectors and lamp proceeds simultaneously with sliding movement of the table on which a patient lies. The smallest thickness of a topographically identifiable layer possible to generate is 0.625 mm. The CAT scanner registers radiological density from 1024 HU to 3071 HU. The scanner's gantry can perform a full rotation in 0.8 seconds. The smallest dimension of a pixel on a CAT scan is 0.19 mm whereas the tomographic reconstruction field must measure at least 96 mm.



Figure 1. BrightSpeed 16 Power Elite CAT scanner

Firstly the 2144715 QA Phantom (the head phantom) manufactured by GE in the United States and used for monthly calibration of CAT scanners (Figure 2) has been analyzed. The casing and geometrical shapes located within the phantom were made from the combination of polymethylmethacrylate and polystyrene and the remaining of the environment has been filled with water. The studies have been performed for the bone scan, one of the most basic computed tomography procedures. The analyzed series consisted of 104 scans. Thickness of a singular layer in the performed imaging procedure was 1.25 mm. Three specific sections of a specific shape were located within the phantom. The first section was a PMMA plate with five holes of a different diameter, the second component was a PMMA plate with six holes of a different diameter arranged diagonally; furthermore, in the second section there was a number of holes of the same diameter arranged in groups of five and located along two sides of the solid body (Ryniewicz et al., 2015). The third section contained 4 identical solid bodies of cylindrical shape arranged in an equal distance from the center of symmetry of the phantom's cross-section.



Figure 2. A head phantom

The subsequent imaging has been performed on the CT Performance Phantom manufactured by GE in the United States (Figure 3). For the purpose of analysis of this phantom the bone scan consisting of 289 scans has been selected. Thickness of the imaging layer was set to 0.625 mm. In case of this phantom four specific sections can be distinguished. The first section consists of cuboid shapes made from a material with a higher radiological density than filling of the phantom, with various dimensions (from 1 to 5 mm), arranged in 11 groups of 1 to 4 shapes each, placed in a semi-circle within the middle of phantom's cross section. The next specific section consists of two plates with a slightly higher radiological density set opposite each other around the periphery of the phantom, in the middle of its length. The other specific section consists of 5 objects with identical circular cross-section with each object made of a material with a different radiological density and the fifth object filled with air. The last specific section consist of 4 rectangular plates arranged in such a manner that each plate is perpendicular to the previous plate and that there are points of high radiological density located along the entire length of the axis of symmetry of the plates.

Detailed measurements has been performed on one selected scan from among 10 scans performed for the head phantom and on one selected scan performed with the use of the specialized phantom.

Materialise Mimics computer program has been utilized to perform geometrical measurements of the shapes located within the phantoms and to measure radiological density in the selected cross-sections. This program has been used to perform digital reconstruction of geometry of the objects on the grounds of the DICOM-format applications and to perform virtual measurement of the characteristic structures reconstructed in 3D.

The performed measurement of radiological density and geometry of the objects in the head and specialized phantoms enabled us to ascertain the measurement uncertainty through use of the A-type method.

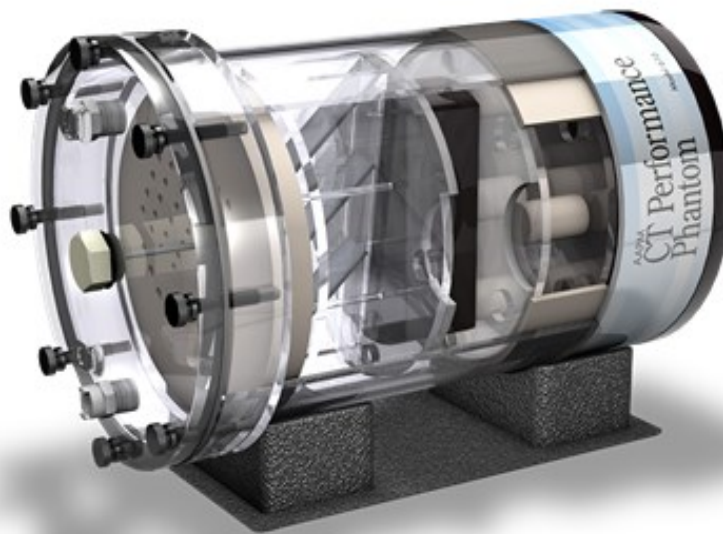


Figure 3. A specialized phantom

3. Study results and discussion

3.1. Measuring radiological density

The Head Phantom

After generating a number of tomography scans performed for the phantoms in the Jan Pawel II Provincial Hospital in Kronso the work started on processing the scans in the Mimics software. Out of the 10 examinations performed in 10 consecutive months on the head phantom the ones in which the greatest number of cross-sections has been created were selected for study. Scans in DICOM format were imported into the Mimics software. The program enables presenting any scan in a horizontal, medial and frontal plane and to reconstruct the image in 3D (Figure 4).

The radiological density measurements were taken in a circular cross-section with the surface of 94.07 mm^2 filled with water in which no other geometrical objects were located. Fifty measurements of radiological density has been taken at the randomly selected points of the cross-section (Figure 5 and 6).

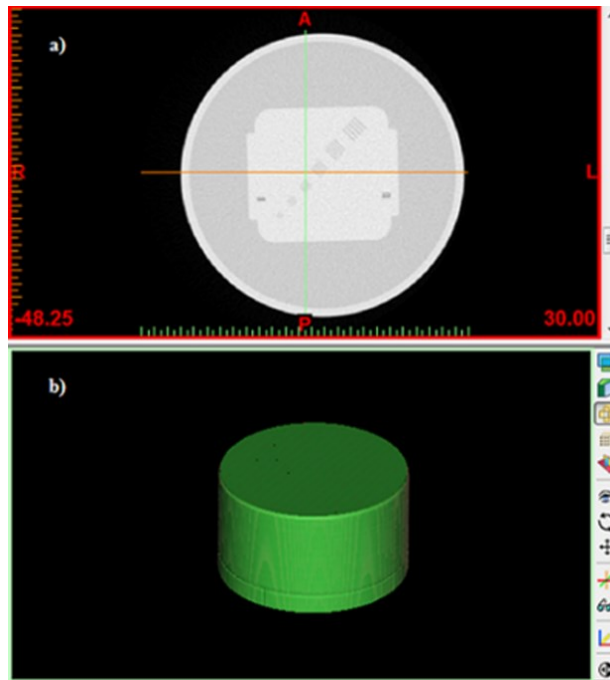


Figure 4. Results of the study of the head phantom: a) horizontal Cross-section layer, b) reconstructed 3D model of the phantom

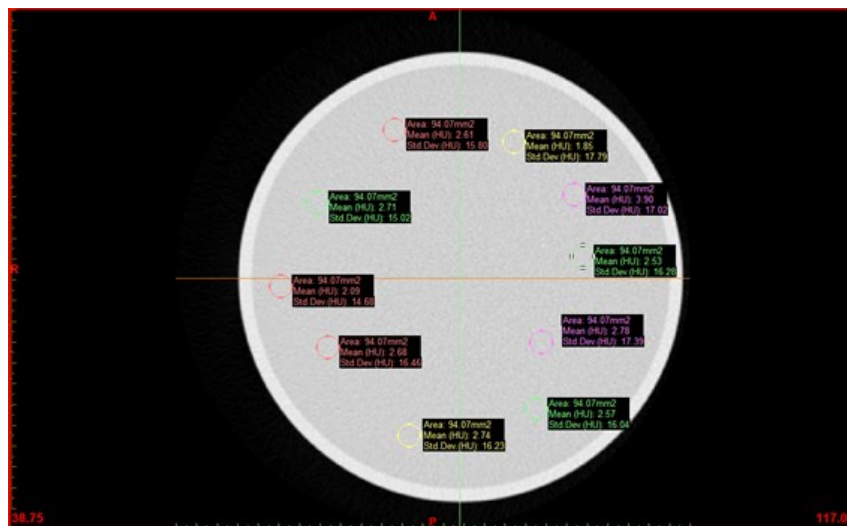


Figure 5. Distribution of the radiological density measurement points on the head phantom

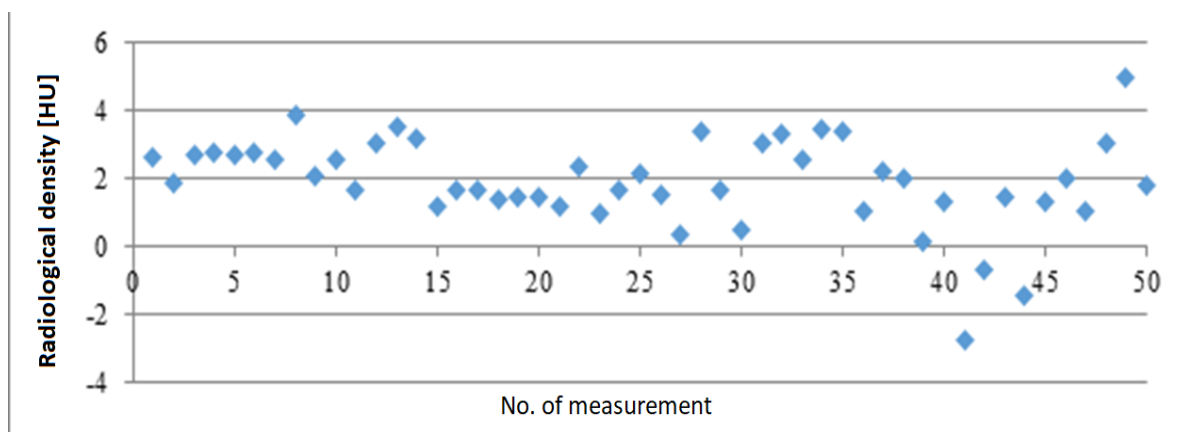


Figure 6. Distribution of radiological density on the horizontal cross-section of the head phantom

The results of the measurements have been subjected to statistical analysis considering such parameters as arithmetic mean, range, median and standard deviation for the experiment.

The calculated statistical parameters for radiological density measurements of the head phantom are, respectively:

- arithmetic mean $\bar{x} = 1,91$ [HU]
- range $R = 7,73$ [HU]
- median $m_e = 1,92$ [HU]
- standard deviation for the experiment $s = 1,34$ [HU]

Results of measurement of calculation uncertainty for the radiological density of the head phantom are as follows:

- standard uncertainty $u = 0,19$ [HU]
- expanded uncertainty $U = 0,38$ [HU]
- final result of measuring $x = 1,91 \pm 0,38$ [HU].

The results of measurements were also displayed in graphical form by creating a histogram along with a superimposed standard distribution curve (Figure 7).

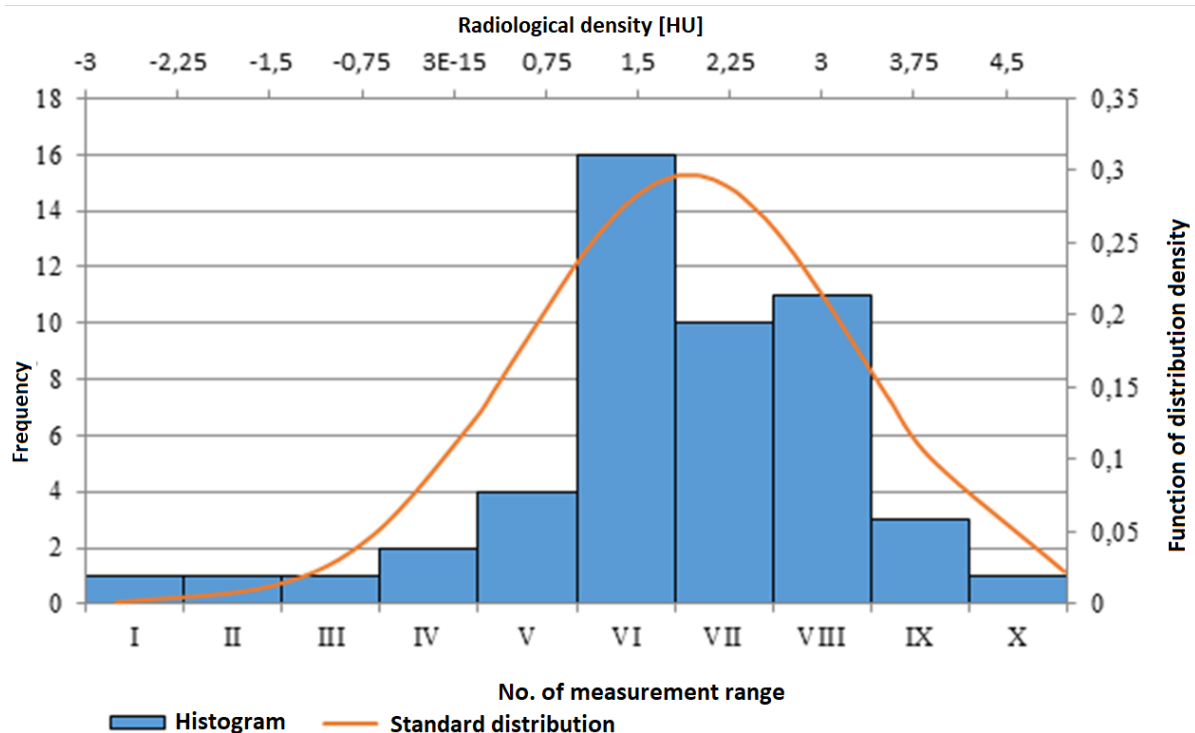


Figure 7. The histogram along with the standard distribution curve of radiological density measurements for the horizontal cross-section of the head phantom

In case of the head phantom histogram the greatest number of measurement results (16) falls onto the range VI whereas the least amount (1 each) is contained in four measuring ranges: I, II, III i X (Figure 7). Analysis of the standard distribution curve indicates that the most probable result of a measurement is the value of 1.85 HU which is contained in range VI which covers the results from the 1.10-1.87 HU range. This consistency is evidence that the generated histogram possess, in fact, the standard distribution and that the measurements do not include errors other than random errors. Distribution of results is a standard distribution which means that the measurement uncertainty overlaps with standard deviation.

The Specialized Phantom

The study of the specialized phantom has been performed during the projection which is routinely performed for patients after application of contrast. Images of three planes as well as a reconstructed 3D model were created in Mimics program.

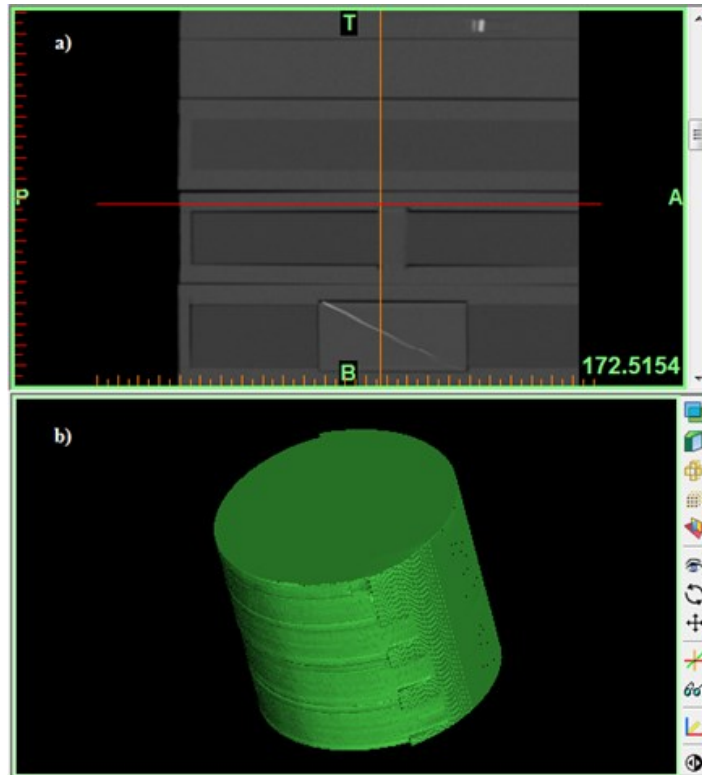


Figure 8. The results of study of the specialized phantom: a) medial plane cross-section, b) reconstructed 3D model of the phantom

The radiological density measurements for the specialized phantom were performed in the horizontal plane, in a circular cross-section with the surface of 89.61 mm^2 in which none additional geometrical shapes were present. Fifty radiological density measurements were taken at the randomly selected points of the cross-section.

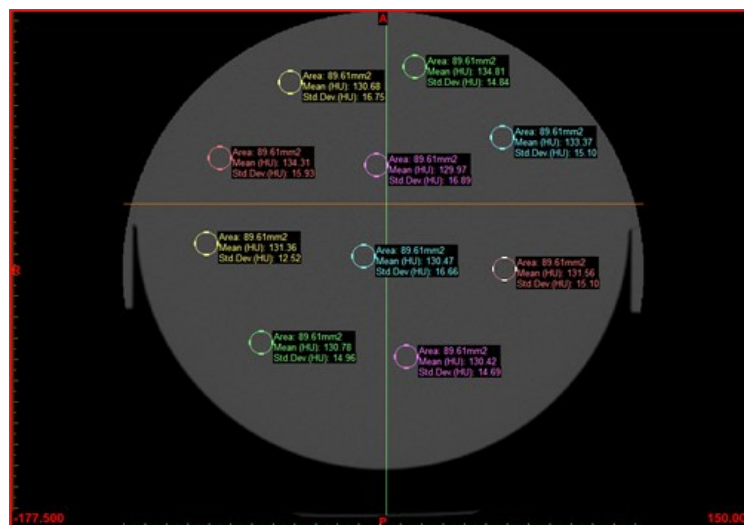


Figure 9. The selected results of radiological density measurements on the horizontal cross-section of the specialized phantom

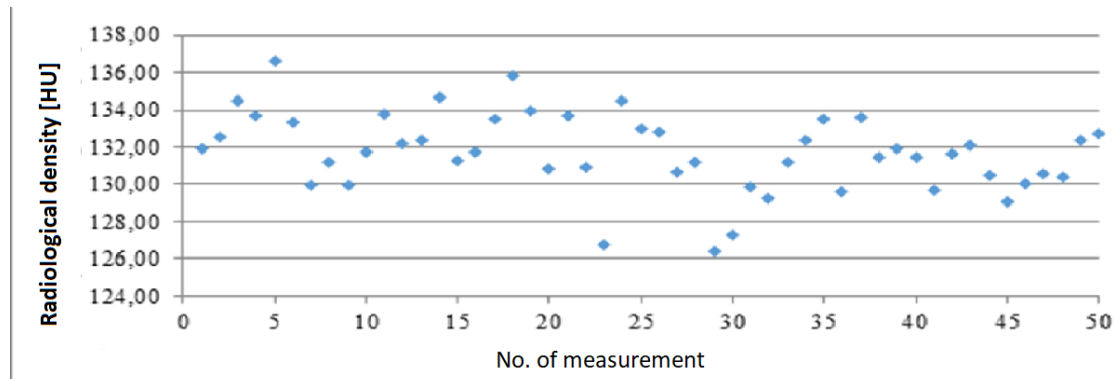


Figure 10. Distribution of radiological density for the horizontal cross-section of the specialized phantom

On the grounds of the collected results the statistical parameters for radiological density have been calculated: arithmetic mean, range, median and standard deviation for the experiment.

The calculated statistical parameters of radiological density measurements for the specialized phantom are as follows:

- arithmetic mean $\bar{x} = 131,72 [HU]$
- range $R = 10,19 [HU]$
- median $m_e = 131,76 [HU]$
- standard deviation for the experiment $s = 2,10 [HU]$

Results of measurement of calculation uncertainty for the radiological density of the specialized phantom are as follows:

- standard uncertainty $u = 0,30 [HU]$
- expanded uncertainty $U = 0,59 [HU]$
- final result of measuring $x = 131,72 \pm 0,59 [HU]$.

The results of calculations were also presented in graphical form by creating a histogram with a superimposed standard distribution curve (Figure 11).

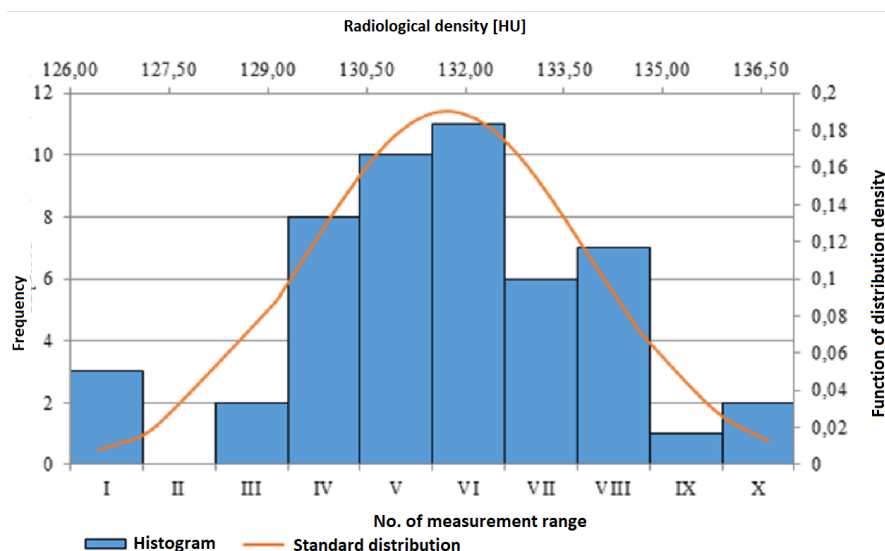


Figure 11. The histogram along with a standard distribution curve for radiological density measurements of the horizontal cross-section of the specialized phantom

In case of the specialized phantom's histogram the greatest number of results is contained within range VI – 11 results (Figure 11). None of the measured values falls onto range II. According to the standard distribution curve the most probable result is the value of 131.74 HU which is contained in range VI which covers values ranging from 131.52 to 132.54 HU. Similarly to the case discussed above the results are the evidence that in the case of the standard distribution of the generated histogram errors are random and standard deviation is equivalent to measurement uncertainty.

3.2. Measuring roundness of cross-sections of phantoms and diameter of holes in the plate

Three measurements of diameter of four holes in the plate located within the head phantom have been performed using Mimics program. The last hole with the diameter of 1 mm has not been measured because it is invisible in the analyzed measurement set. Average results of measuring of the consecutive holes are: 9.99 mm, 7.52 mm, 5.01 mm and 3.02 mm whereas the nominal diameters of the holes are: 10.00 mm, 7.50 mm, 5.00 mm and 3.00 mm. In comparison to the nominal values the measuring errors for the diameter measuring did not exceed 5%.

In order to determine roundness of both phantoms measurements have been taken of the outer diameter of the cylindrical casing at the horizontal cross-section (Figure 12). Three measurements of the diameter for each cross-section have been performed for both phantoms. These measurements indicated that the head phantom is of a circular shape. Study of the diameter of cross-section of the specialized phantom did not confirm circular shape and instead indicated elliptical shape.

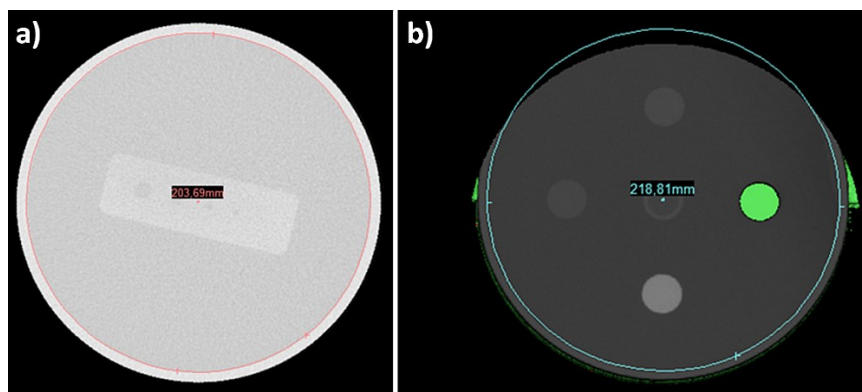


Figure 12. The exemplary measurements of cross-sections' diameter on the horizontal plane: a) the head phantom, b) the specialized phantom

3.3. Measuring geometry of objects placed within phantoms with estimation of measurement uncertainty

The head phantom

Fifty measurements of the rectangular plate have been taken using the reconstructed 3D model of the head phantom.

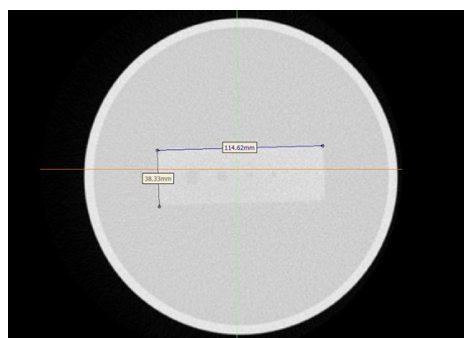


Figure 13. Measurements of length and width of the plate located within the head phantom

Statistical parameters, measurement uncertainty and the final measurement results have been calculated on the grounds of the results of measurements (Table 1).

Table 1
Results of measurements of length and width of the plate located within the head phantom

Statistical parameter	Plate width [mm]	Plate length [mm]
arithmetic mean, \bar{x}	37.81	114.77
Standard deviation for the experiment, s	0.27	0.35
Range, R	1.49	1.70
Median, m_e	37.81	114.63
standard uncertainty, u	0.04	0.05
expanded uncertainty, U	0.08	0.10
Final results of measurements, x	37.81 ± 0.08	114.77 ± 0.10

Histograms along with standard distribution curves have been developed for both dimensions of the plate (Figure 14 and 15).

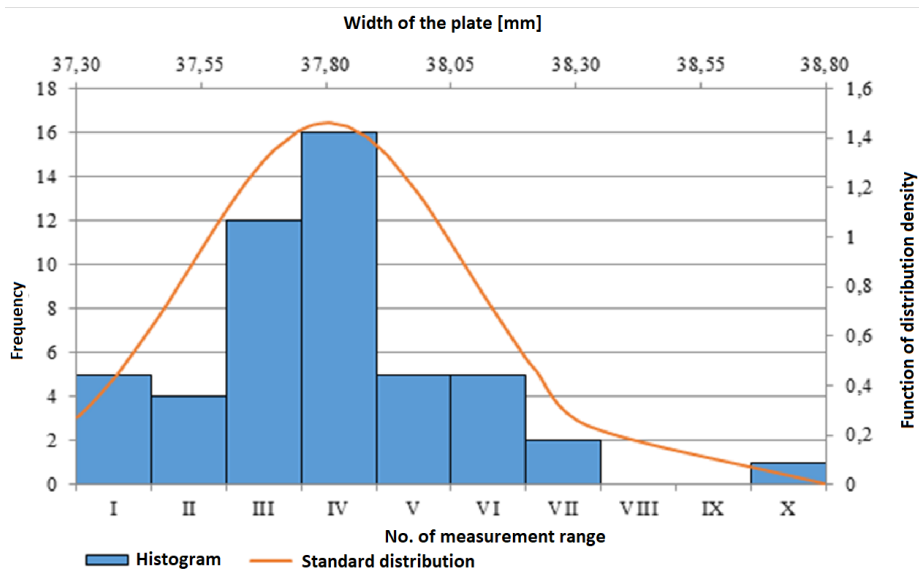


Figure 14. The histogram with standard distribution curve for results of measuring of width of the plate

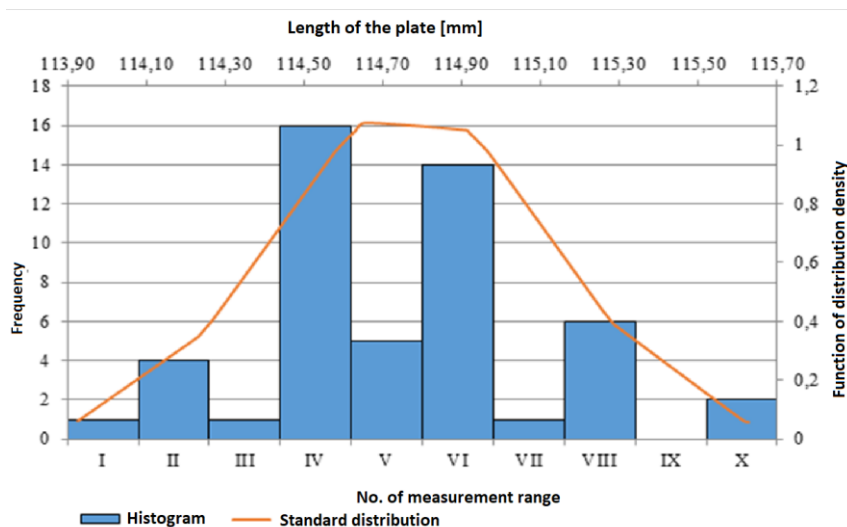


Figure 15. The histogram with standard distribution curve for results of measuring of length of the plate

For plate's width histogram the greatest number of measurement results – 16 – is contained within range IV. There are no measurements corresponding with the values from ranges VIII and X. The calculated standard distribution indicates that the most probable measurement result is the value of 37.81 mm. This results falls onto range IV – which covers values from 37.75 to 37.90 mm. Accuracy of the results allows us to ascertain that this histogram possesses, in fact, a standard distribution and that the mistakes made by the operator during taking measurements did not significantly influence the results. In this case measurement uncertainty is equivalent to standard deviation because the results are distributed in the standard manner.

Also in the case of the histogram with the standard distribution curve for measurements of length of plate the number of results is 16 and is contained within range IV. A singular result has been recorded in ranges I, II and VII whereas there are no results for range IX. In this case calculations indicate that the most probable result for measurement of plate's length is the value of 114.66 mm which does not fit in range IV but in range V instead which covers values from 114.61 to 114.78 mm. The differences prove that the distribution of the generated histogram is not a standard distribution and apart from the random errors also mistakes made by the operator significantly influenced the results of measurements. It can be inferred from the shape of the graph that the results are not distributed in a standard manner because the curve does not take the classic bell-like shape and as a result in this case the standard deviation cannot be equated with measurement uncertainty.

The specialized phantom

Measurements have been taken of one of the four cuboid shapes located within the specialized phantom by using reconstructive cross-sections of the phantom. Length and height of the object were measured on the medial plane whereas width of the object was measured on the horizontal plane. Each dimension has been measured 50 times. Width has been marked with letter A, length with letter B and height with letter H. A 15 mm transverse cross-section and 74.34 mm of medial cross-section have been selected for taking measurements.

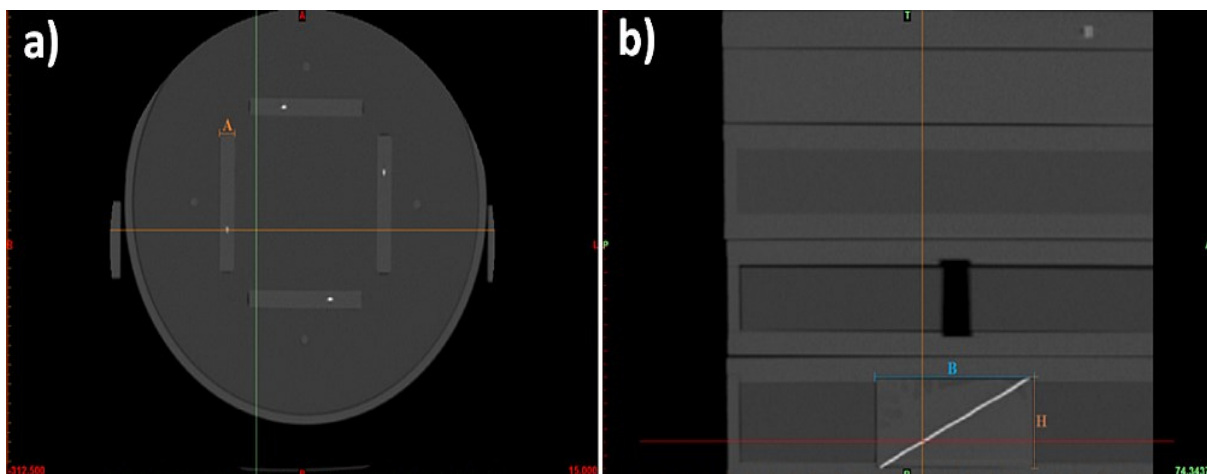


Figure 16. Specialized phantom's cross-sections: a) horizontal with width of the measured object marked, b) medial with length and height of the object marked

Measurements for each dimensions have been subjected to statistical analysis (Table 2).

Table 2

Results of the statistical analysis of measurements of width (A), length (B) and height (H) of the cuboid

Statistical parameter	Plate width (A) [mm]	Plate length (B) [mm]	Plate height (H) [mm]
arithmetic mean, \bar{x}	9.54	72.13	34.73
Standard deviation for the experiment, s	0.17	0.26	0.30
Range, R	0.66	1.48	1.24
Median, m_e	9.49	72.15	34.84
standard uncertainty, u	0.02	0.04	0.04
expanded uncertainty, U	0.05	0.07	0.09
Final result of measurement, x	9.54 ± 0.05	72.13 ± 0.07	34.73 ± 0.09

Analogously to geometrical measurements of the head phantom the histograms of the specific measurements of the cuboid located within the specialized phantom have been prepared on the grounds of the gathered results; standard distribution curves were superimposed over these histograms (Figures 17-19).

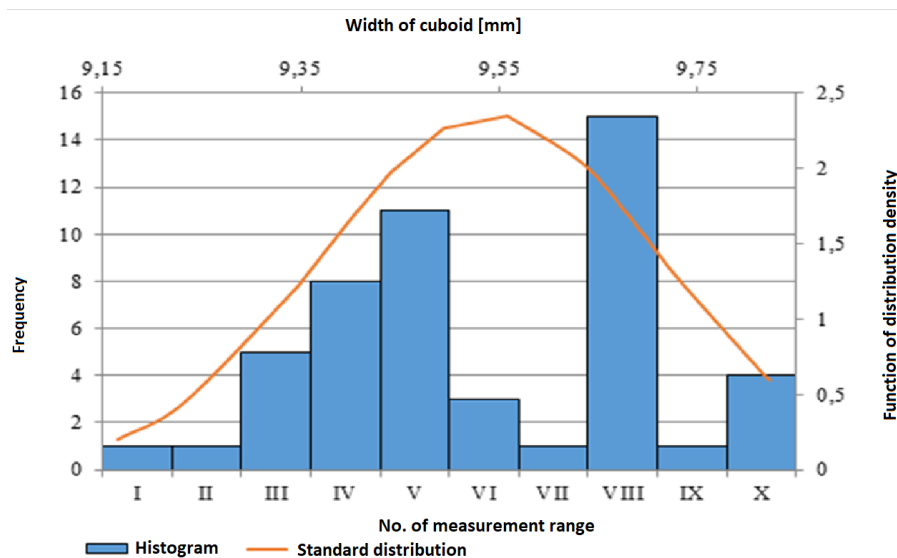


Figure 17. The histogram and standard distribution curve for measurements of width (A) of the cuboid

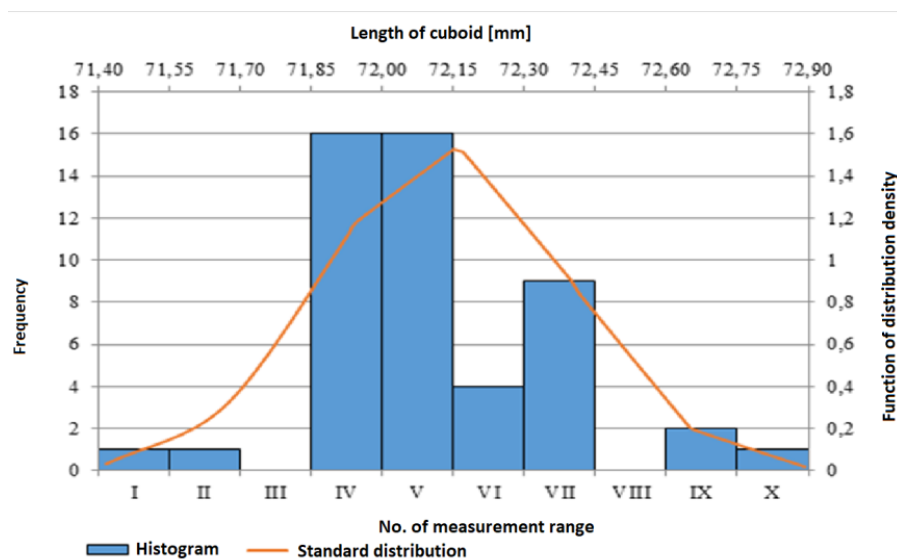


Figure 18. The histogram and standard distribution curve for measurements of length (B) of the cuboid

The greatest number of results for width (A) measurement is contained in range VIII; the value is 15. A singular result has been recorded in four measuring ranges: I, II, VII i IX. According to the calculated standard distribution the most frequent result should be the value of 9.56 mm; however, this value does not fit in range VIII but instead in range VI which covers values from 9.50 to 9.57 mm. The demonstrated differences indicate that in reality the distribution of results of width's measurement of the cuboid is not the standard distribution and the results were influenced by human errors and other random errors. In relation to the above fact the standard distribution most certainly cannot be equated with the measurement uncertainty for object's width measurements. The distribution of the results demonstrated by the histogram is a bi-modal distribution which means that on the generated density function graph there are two distinct peaks. In this case they appear in measurement ranges V and VIII. Such distribution of the results can be an effect of a human factor (operator's) error during measuring the width (A) of the cuboid – e.g. as a result of marking the beginning and/or end of the operating distance incorrectly.

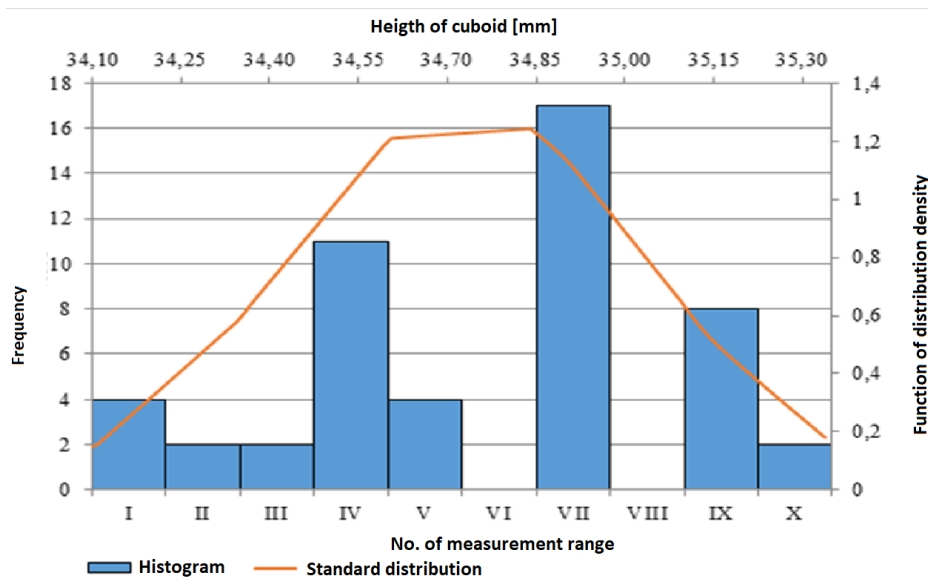


Figure 19. The histogram along with standard distribution curve for measurements of height (H) of the cuboid

For measurements of length (B) of the cuboid (Figure 18) the majority of the results is contained in two ranges: IV and V – with 16 measured values in each range. In turn, the measurements for cuboid's length did not appear within ranges III and VIII. On the grounds of the calculated standard distribution the most probable result is the value of 72.15 mm which falls on range V which covers values from 72.01 to 72.16 mm. The shape of the produced curve does not exactly resemble the characteristic bell-like shape of the standard distribution but the determined value falls within range V.

Over the course of analysis of the height (H) measurements it has been ascertained that the greatest number of results, 17, falls within range VII of the histogram (Figure 19). The calculated values of standard distribution indicate that the most probable result for height measuring is the value of 34.84 mm. However, also in this case the produced shape of the curve does not resemble the characteristic bell-like shape and the calculated values fall on the extremes of the measuring consistency. Similarly to the cuboid's width (A) histogram the results of height (H) measuring have a bi-modal distribution and the maximum values were reached in ranges IV and VII. Also for these measurements the most likely cause behind the produced distribution of measurement results are human factor errors as well as the errors resulting from construction of the detector array.

4. Conclusions

The performed analysis of the accuracy of internal structure and shape mapping of the head phantom and the specialized phantom enabled us to ascertain the possible source of measurement errors in CT imaging. By utilizing appropriate tools for numerical processing 3D models for both phantoms have been modeled in Mimics program. Fifty measurements of radiological density were performed in the randomly determined areas of the selected cross-sections of the phantoms. In accordance with properties of the master models the radiological density in these areas should take uniform values. The performed measurements confirmed appropriate distribution of radiological density. The statistical analysis of the radiological density measurements confirmed that random errors constitute the primary group of measurement errors for both head and specialized phantoms. For the majority of radiological density measurements the distribution of results is consistent with standard distribution,

Proper distribution of radiological density achieved during tests concerning correct functioning of a CAT scanner is pivotal for CT patient's diagnostics. Nonhomogeneous radiological density within structure of the tissues with the same X-ray radiation absorption properties could mislead a diagnostician. As a result artifacts could be displayed in the healthy tissue.

Roundness of both phantoms has been examined using horizontal cross-sections and it has been indicated that the head phantom is round whereas the specialized phantom is elliptical in shape. Measurements were also taken of the diameter of the head phantom and four holes in the plate placed within this phantom. The geometry of two three-dimensional objects located within phantoms and made of materials with a different radiological density than the surrounding environment has been examined. In case of the head phantom the length and width of the plate visible in imaging have been measured 50 times. The same amount of measurements has been performed for the dimensions of the cuboid – width, length and height were all measured. These measurements were taken using horizontal and sagittal cross-sections.

Estimation of the measurement uncertainty of the geometry of the objects within the phantoms indicated that during measuring linear parameters operator errors, which are primary caused by resolution of the sight organ, occur apart from random errors.

Errors in shape reproduction of tissue structures, which can be detected on the grounds of the analysis of phantom's geometry reproduction, could possibly distort objective, factual and natural 3D structures and lead to diagnostic errors and even to mistakes in planning surgeries. The performed studies of the quality of master model reproduction indicate that the highest values of shape reproduction errors occur during assessment of irregular rounded objects (Ryniewicz, 2013).

The results of measuring of radiological density and geometry of 3-dimensional shapes located within phantoms were utilized to perform full statistical analysis. For each of the studied values an arithmetic mean, range and standard deviation were calculated; furthermore measuring uncertainty was estimated using type-A method. For the radiological density measurements the standard measurement uncertainty was 0.19 HU and 0.30 HU for the head phantom measurements and specialized phantom measurements respectively. The calculated expanded uncertainty is, respectively: 0.38 HU and 0.59 HU. The measured values of standard and expanded measurement uncertainty for width and length of the plate in the head phantom were 0.04 mm (width)/0.08 mm (length) and 0.05 (width)/0.10 mm (length) respectively. The uncertainty for dimensions of the cuboid located inside the specialized phantom has been calculated. Standard uncertainty and expanded uncertainty for width, length and height of the cuboid were 0.02/0.04 mm, 0.04/0.07 mm and 0.04/0.09 mm respectively. The results of the performed measurements were displayed in graphical form as histograms over which standard distribution curves were superimposed. For radiological density measurements the standard deviation also represents their measurement uncertainty. The achieved values of deviation for head and specialized phantom were 1.34 HU and 2.10 HU respectively. It means that the limit values of ± 4 HU were not exceeded and that the guidelines indicated in Regulation of Health Minister concerning uniform image zone were met in studies on both tomographic phantoms.

The measured values of expanded uncertainty did not exceed 1 HU and the maximum range from 50 measurements was 10 units in Hounsfield scale which in comparison to the whole range of the scale is statistically irrelevant; thus the phantoms can be used to calibrate uniformity of tomographic image. Values of standard deviation for radiological density measurements did not exceed the limit value which means that the examined CAT scanner meets the requirements regarding uniformity of imaging and noise level stipulated in Regulation of Minister of Health.

Mimics program is a universal tool for measuring radiological density in tomography scans and accuracy of shape reproduction in CT imaging. The proposed procedure is significant owing to the adopted measuring strategy for the target device but can also serve as a tool for comparing quality of various CAT scanners.

References

- Akpochafor, M.O., Adeneye, S.O., Ololade, K., Omojola, A.D., Adedewe, N., Adedokun, A., Aweda, M.A., Aboyewa, O.B. (2019). Development of computed tomography head and body phantom for organ dosimetry. *Iranian Journal of Medical Physics*, 16(1), 8-14.
- Bolstad, K., Flatabø, S., Aadnevik, D., Dalehaug, I., Vetti, N. (2018). Metal artifact reduction in CT, a phantom study: subjective and objective evaluation of four commercial metal artifact reduction algorithms when used on three different orthopedic metal implants. *Acta Radiologica*, 59(9), 1110-1118.
- De Oliveira, M.V., Wenzel, A., Campos, P.S., Spin-Neto, R. (2017). Quality assurance phantoms for cone beam computed tomography: a systematic literature review. *Dentomaxillofacial Radiology*, 46(3).
- Filippou, V., Tsoumpas, C. (2018). Recent advances on the development of phantoms using 3D printing for imaging with CT, MRI, PET, SPECT, and ultrasound. *Medical Physics*, 45(9), e740-e760.
- Haleem, A., Javaid, M. (2020). 3D printed medical parts with different materials using additive manufacturing. *Clinical Epidemiology and Global Health*, 8(1), 215-223.
- Hermanek, P., Carmignato, S. (2017). Porosity measurements by X-ray computed tomography: Accuracy evaluation using a calibrated object. *Precision Engineering*, 49, 377-387.
- Higaki, T., Nakamura, Y., Zhou, J., Yu, Z., Nemoto, T., Tatsugami, F., Awai, K. (2020). Deep learning reconstruction at CT: phantom study of the image characteristics. *Academic Radiology*, 27(1), 82-87.
- Holmes, R.B., et al. (2020). Creation of an anthropomorphic CT head phantom for verification of image segmentation. *Medical Physics*, 47(6), 2380-2391.
- Jahnke, P., Schwarz, F.B., Ziegert, M., Almasi, T., Abdelhadi, O., Nunninger, M., Hamm, B., Scheel, M. (2018). A radiopaque 3D printed, anthropomorphic phantom for simulation of CT-guided procedures. *European Radiology*, 28(11), 4818-4823.
- Jahnke, P., Schwarz, S., Ziegert, M., Schwarz, F. B., Hamm, B., Scheel, M. (2019). Based 3D printing of anthropomorphic CT phantoms: Feasibility of two construction techniques. *European Radiology*, 29(3), 1384-1390.
- Norma PN-EN ISO 2919:2014-12. Ochrona radiologiczna -- Zamknięte źródła promieniotwórcze -- Wymagania ogólne i klasyfikacja.
- Norma PN-ISO 14146:2006. Ochrona radiologiczna -- Kryteria i granice zdolności pomiarowych dla okresowej oceny laboratoriów pomiaru dawek indywidualnych promieniowania rentgenowskiego i gamma.
- Norma PN-ISO 9978:1999. Ochrona radiologiczna -- Promieniotwórcze źródła zamknięte -- Metody badania szczelności.
- Resolution of Minister of Health of 18th of February 2011 regarding conditions for safe application of ionizing radiation for all types of medical exposure (JoL 2011, No. 51, item 265).
- Ryniewicz, A. (2013). *Ocena dokładności odwzorowania kształtu powierzchni elementów biologicznych w badaniach in vivo oraz in vitro*. Prace Naukowe Politechniki Warszawskiej. Mechanika.

- Ryniewicz, A., Ostrowska, K., Knapik, R., Ryniewicz, W., Krawczyk, M., Śladek, J., Bojko, Ł. (2015). Ocena odwzorowania wybranych parametrów geometrycznych w tomografii komputerowej z zastosowaniem wzorców. *Przegląd Elektrotechniczny*, 91(6), 88-91.
- Ryniewicz, W., Ryniewicz, A., Bojko, Ł. (2019). Geometrical parameters of the mandible in 3D CBCT imaging. *Biocybernetics and Biomedical Engineering*, 39(2), 301-311.
- Sahbaee, P., Segars, W.P., Marin, D., Nelson, R.C., Samei, E. (2017). The effect of contrast material on radiation dose at CT: Part I. Incorporation of contrast material dynamics in anthropomorphic phantoms. *Radiology*, 283(3), 739-748.
- Shim, S., Saltybaeva, N., Berger, N., Marcon, M., Alkadhi, H., Boss, A. (2020). Lesion Detectability and Radiation Dose in Spiral Breast CT With Photon-Counting Detector Technology: A Phantom Study. *Investigative radiology*, 55(8), 515-523.
- Si-Mohamed, S., Bar-Ness, D., Sigovan, M., Tatard-Leitman, V., Cormode, D.P., Naha, P.C., Coulon, P., Rasclé, L., Roessl, E., Rokni, M., Altman, A., Yagil, Y., Boussel, L., Douek, P. (2018). Multicolour imaging with spectral photon-counting CT: a phantom study. *European Radiology Experimental*, 2(1), 1-10.
- Subhas, N., Pursyko, C.P., Polster, J.M., Obuchowski, N.A., Primak, A.N., Dong, F.F., Herts, B.R. (2018). Dose reduction with dedicated CT metal artifact reduction algorithm: CT phantom study. *American Journal of Roentgenology*, 210(3), 593-600.
- Tino, R., Yeo, A., Leary, M., Brandt, M., Kron, T. (2019). A systematic review on 3D-printed imaging and dosimetry phantoms in radiation therapy. *Technology in cancer research & treatment*, 18.
- Turek, P., Budzik, G., Przeszłowski, Ł. (2020). Assessing the Radiological Density and Accuracy of Mandible Polymer Anatomical Structures Manufactured Using 3D Printing Technologies. *Polymers*, 12(11), 2444.
- Villarraga-Gómez, H., Herazo, E.L., Smith, S.T. (2019). X-ray computed tomography: from medical imaging to dimensional metrology. *Precision Engineering*, 60, 544-569.
- Wu, R.Y., Liu, A.Y., Williamson, T.D., Yang, J., Wisdom, P.G., Zhu, X.R., Frank, S.J., Fuller, C.D., Gunn, G.B., Gao, S. (2019). Quantifying the accuracy of deformable image registration for cone-beam computed tomography with a physical phantom. *Journal of Applied Clinical Medical Physics*, 20(10), 92-100.
- Yasaka, K., Akai, H., Mackin, D., Court, L., Moros, E., Ohtomo, K., Kiryu, S. (2017). Precision of quantitative computed tomography texture analysis using image filtering: a phantom study for scanner variability. *Medicine*, 96(21), e6993.